Chapter 3

Categorization of Topologies based on Product Distributions and Cage-Defining Rings

In this chapter, the discussion part (investigation of the obtained product distributions, correlation to the cage topologies, introduction of a new geometric concept, cage-defining ring) of Part I of my thesis is presented. This chapter is a combined reconstitution of two of my publications: J. H. Kang et al., ChemPhysChem 2018, 19, 412 and J. H. Kang et al., ACS Catal. 2019, DOI: 10.1021/acscatal.9b00746. The majority of this chapter is adapted from the Result and Discussions part of my ACS Catalysis paper, but further augmented with the contents from my ChemPhysChem paper.

3.1. Introduction

The last chapter demonstrated the MTO time-of-stream data which show transient selectivity behaviors of 30 catalysts investigated in this work. A global pattern of the influence of topology on MTO product selectivity did exist. At a fixed temperature 400 °C, topologies could be grouped into 4 categories based on their product distributions. The first category gave almost one-to-one ethylene-to-propylene selectivity ratios. The second and third categories showed ethylene- and propylene-dominant product selectivity distribution patterns, respectively. The fourth category of topologies possessing the LTA cages in common yielded high butylene selectivities. This categorization of topologies was possible because those product distributions were primarily dependent on the cage topology rather than the elemental composition.

In this chapter, the MTO product distributions will be revisited on the basis of overall selectivities evaluated in the range of the maximum conversion of methanol (98–100%). The concept of cage-defining and its size which show a strong correlation to the four types of topologies will be introduced. A graphic abstract which summarizes the contents of this chapter is shown in Figure 3.1.

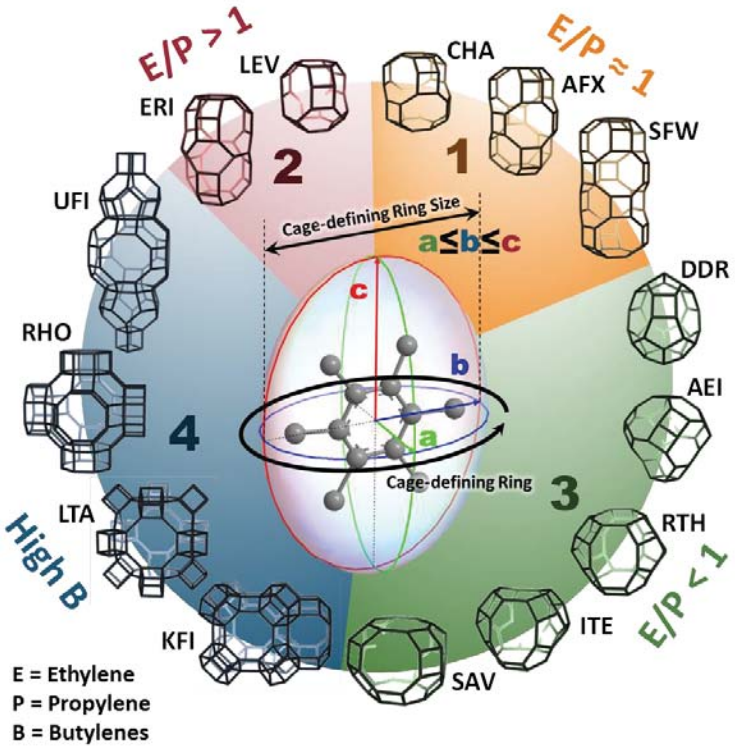

Figure 3.1. Schematic illustrations of 14 small-pore/cage topologies which were classified into four categories based on their olefin product distributions and the concept of the cage-defining ring.

3.2. Categorization of Topologies

On the basis of olefin selectivity distributions, the investigated topologies could be classified into the four groups as follows:

At the MTO reaction temperature of 400 °C,

- Category I: group of CHA, AFX, SFW, SSZ-99, and SSZ-104 which show even-balanced ethylene-to-propylene ratios close to unity. (E/P ~ 1)
- Category II: group of LEV, ERI, and SSZ-105 which show ethylene selectivities higher than propylene selectivities. (E/P > 1)
- Category III: group of DDR, AEI, RTH, ITE, and SAV which show propylene selectivities higher than ethylene selectivities. (E/P < 1)
- Category IV: group of LTA, RHO, KFI, and UFI which show no clear pattern of ethylene-to-propylene, but high butylenes selectivities with the LTA cages as their major cages in common.

3.2.1. Ethylene-to-Propylene Ratio

The product distributions from MTO reactions conducted at 400 °C were illustrated as bar charts in this chapter, as shown in Figures 3.2–3.5, and representing selectivity values were obtained by averaging selectivities of products in the range of 98–100% of methanol conversion.

Category I Figure 3.2. (a) shows the MTO product distributions of four CHA-type isostructural catalysts. Apparently, these CHA-type catalysts yielded strikingly similar product distributions despite completely different elemental compositions. The overall ethylene-to-propylene ratios were close to 1-to-1 at 400 °C. These results strongly support that the cage geometry plays the most important role in determining the resultant olefin

product ratio from MTO reaction. Also, these CHA-type catalysts showed the highest ethylene and propylene selectivities (85–90 %) among all tested topologies in this work and low butylenes selectivities (< 10 %), as mentioned in the previous chapter.

The only three frameworks that are built exclusively with parallel arrays of d6r composite building units are CHA, AFX, and SFW belonging to the ABC-6 family, as mentioned in the previous chapter.[16, 91] In terms of the methanol-accessible regions within cages (see Figure A5), the cage length order is CHA (6.8 Å) < AFX (11.5 Å) < SFW (15.6 Å). In spite of this serious size difference, the ethylene-to-propylene ratios of these three types of cages were close to unity regardless of the elemental composition as shown in Figure 3.2(b). The AFX-type zeolite shown here is the high silica (Si/Al = 14.7) sample. The cage size order was the same to the total alkane selectivity ($C_{2–4}$) order and the initial propane selectivity order, regardless of elemental compositions. For the zeolite series, the total alkane selectivity order was 9.6 % for SSZ-13, 30.5 % for SSZ-16, and 48.8 % for SSZ-52, respectively. This sequence was the same to the case of SAPO-series (4.8 % for SAPO-34 < 13.1 % for SAPO-56 < 20.7 % for STA-18). The initial propane selectivity sequence of the zeolite series was 11.9 % for SSZ-13, 47.2 % for SSZ-16, and 71.5 % for SSZ-52, respectively. This order was the same to the total alkane order since the majority of produced alkane species was propane which is predominantly produced at the beginning stage of all reactions. The SAPO-series showed the same sequence (8.0 % for SAPO-34 < 14.8 % for SAPO-56 < 19.5 % for STA-18) for the initial propane selectivity.

The extension of the CHA-AFX-SFW series eventually reaches the GME framework. GME has straight 12-membered ring channels which is a topological result of its AABB stacking. (i.e., the 12-ring channel of GME can be seen as an extra-long cage having an infinite length.) However, large-pore zeolitic frameworks such as GME cannot hold the hydrogen pool intermediates of MTO reaction. And furthermore, thermally instable GME zeolite undergo a phase transition to another 12-ring framework AFI at a high temperature

over ca. 280 °C.[92] SSZ-99 and SSZ-104 are the CHA-GME intergrown zeolites.[75-76] In these zeolites, CHA-portions form 'end closures' for intergrown GME portions, and the GME-to-AFI phase transformation was not observed. Also, there are still active CHA-type cages just like SSZ-13. Therefore, it is predictable that SSZ-99 and SSZ-104 will also show ethylene-to-propylene ratios close to one. Indeed, although their Si/Al ratios were low and lifetimes were short, these two zeolite yielded ethylene-to-propylene ratios close to unity as shown in Figure 3.2(c). High initial propane selectivities (63.6 % for SSZ-99 and 62.9 % for SSZ-104) were observed probably due to the high density of paired Al-sites originated from low Si/Al ratios of these zeolites.[64]

Category II LEV and ERI form the second category of topology on the basis of ethylene-to-propylene ratios. As demonstrated in the previous chapter, most of the catalysts belonging to this category yielded transient ethylene selectivities higher than propylene except for SAPO-35. Figure 3.3 illustrates overall product selectivity distributions of all catalysts in this category. The MTO data of SAPO-17 performed at 375 °C and 425 °C were adapted from a work reported by Wilson and Barger in 1999.[44]

Among all topologies demonstrated in this work, LEV has the smallest cages. There are several known topologies which have minor cages smaller than LEV-type cages. However, such cages are not capable of accommodating hydrogen pool intermediate species. Deimund et al. reported that ERS-7 (ESV), MCM-35 (MTF), SAPO-39 (ATN) and RUB-37 (CDO) showed very poor or almost no MTO activity at 400 °C and that no significant amount of occluded aromatic species was detected in the used catalysts.[87] Therefore, one can conclude that the LEV-cage is practically the lowest limit in size for the MTO reaction. The Liu group at the Dalian Institute of Chemical Physics (DICP) confirmed that no significant amount of fully-substituted hydrogen pool species was formed in LEV-type catalysts (SAPO-35 and RUB-50) on the basis of the *in situ* solid-state ^{13}C NMR technique.[33-34]

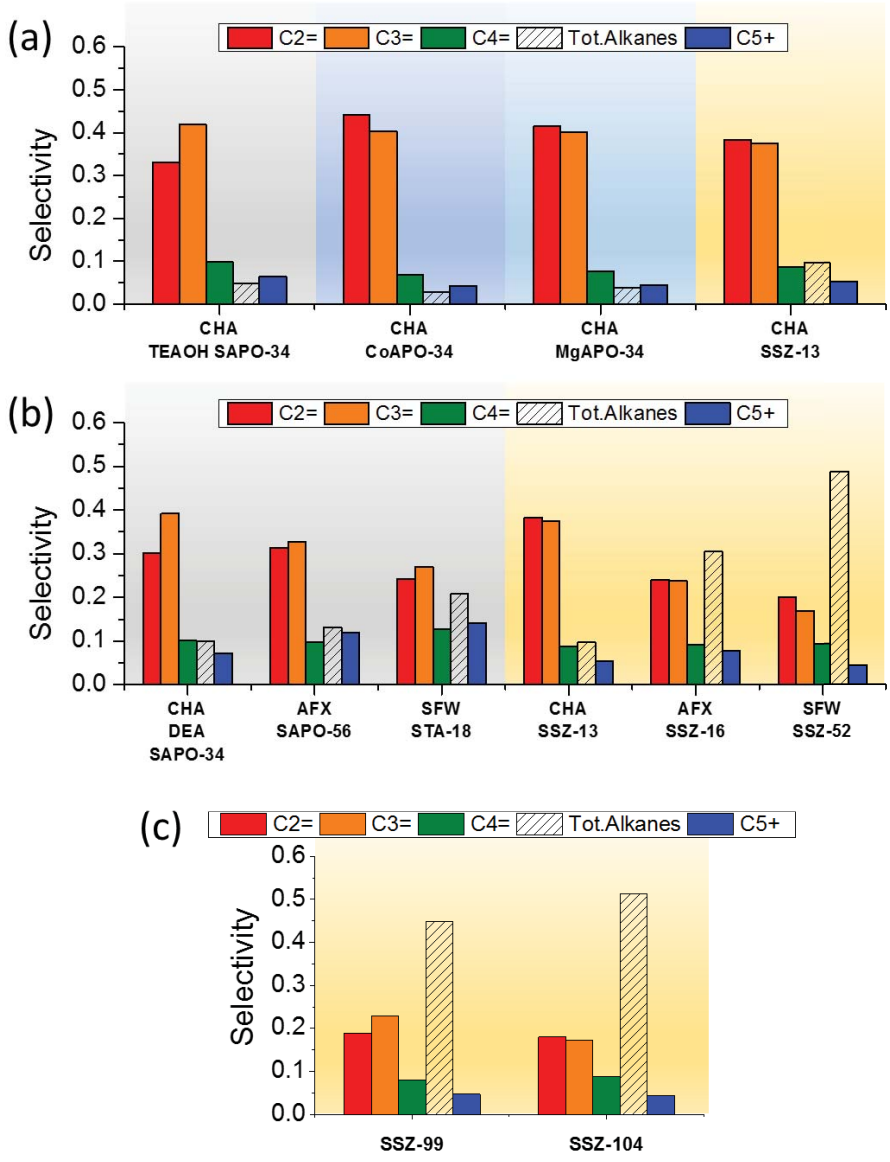

Figure 3.2. MTO product distributions when the methanol conversion is in the range of 98–100%: (a) four isostructural CHA-type molecular sieves, (b) two CHA-AFX-SFW series as SAPOs and zeolites, and (c) two CHA-related GME-intergrown ABC-6-type zeolites. The reactions are performed at T = 400 °C and WHSV(MeOH) = 1.3 h^{-1}.

Inasmuch as higher olefins are produced by aromatic intermediates having more and longer side chains,[37] it can be concluded that the confinement effect of small LEV cages is the main reason why ethylene and propylene are the main products of MTO reaction over LEV-type catalysts.

As demonstrated in the previous chapter, the two LEV zeolites synthesized from two different OSDAs having different Si/Al ratios produced more ethylene than propylene at all stages of reactions. It was reported that a LEV-type zeolite from another OSDA, 1-adamantylamine, also gave ethylene as the major MTO product.[32] On the other hand, SAPO-35 showed a higher propylene selectivity than its ethylene selectivity despite the fact that SAPO-35 is a LEV-type molecular sieve. It is known that the ethylene-to-propylene ratios of SAPO-35 are depending on the Si-contents of the catalyst. Pinilla-Herrero et al. reported that the formation of islanded Si-sites is responsible for this trend and that SAPO-35 indeed produced more ethylene than propylene when Si/T ratio was higher than 0.140.[38] Interestingly, the transient ethylene-to-propylene ratio kept increasing with time of stream. As shown in Figure 2.15 in the previous chapter and Figure A9, the transient ethylene-to-propylene ratio was initially 0.80, but increased to 1.30 within an hour. However, the deactivation of SAPO-35 happened much earlier than that. This short lifetime of SAPO-35 is, as explained in the previous chapter, because of its large size of crystals (20–30 μm) and low-dimensional (2D) channel system. Most of MTO data of SAPO-35 in the literature show similarly short lifetimes of catalysts.[38-39, 46, 93] As shown in Figure A9, the other LET and ERI-type catalysts also show sharply increasing transient ethylene-to-propylene ratios with time of stream, and deactivation occurs after the transient ratios became higher than unity. Also, this increasing trend of transient ethylene-to-propylene ratio was observed only from LEV and ERI-type catalysts. Other common MTO catalysts (CHA or AEI) did not show this type of rapidly increasing ethylene-to-propylene ratios, as illustrated in Figure A9. The origin of this behavior may be related to the transport (diffusion) processes within the porous

crystals,[94] but it is still not clear due to a lack of experimental evidence. Further investigation is required.

ERI is the other member of Category II. In terms of the methanol-accessible space (see Figure A6), an ERI cage (10.7 Å) is longer than a CHA cage (6.8 Å) and slightly shorter than an AFX cage (11.5 Å). But in terms of the diameter of the largest sphere that can be included, ERI (7.04 Å) is even narrower than LEV (7.10 Å). As shown in the previous chapter and Figure 2.15, SSZ-98 showed a very high overall ethylene-to-propylene ratio of 1.46 (transient maximum = 2.07). Other intergrown zeolites having ERI-type cages, such as ZSM-34 (ERI/OFF intergrowth)[95] or SSZ-105 (ERI/LEV intergrowth, this work) showed similarly high ethylene selectivities at 400 °C. These results strongly support the idea that the geometry of ERI-cage plays a crucial role to produce ethylene with high selectivity.

SAPO-17 is another ERI-type molecular sieve that gives very high ethylene selectivity. Wilson and Barger at UOP reported the ethylene-to-propylene ratios of 1.1 and 2.0 at 375 °C and 425 °C, respectively.[44] A similar result was reported by Nawaz et al. at 425 °C.[52] Although these experiments were not conducted at 400 °C which is the standard temperature of this work, many works concluded that higher ethylene-to-propylene ratios can be achieved at higher reaction temperature within a temperature range of 350–450°C.[32, 44, 46, 67, 88, 96] (Different reaction mechanisms undergo outside this temperature range.[13]) Therefore, on the basis of intrapolation, it can be deduced that, at 400 °C, the expected ethylene-to-propylene ratio from SAPO-17 will be approximately 1.4 to 1.5, which resembles the value from SSZ-98.

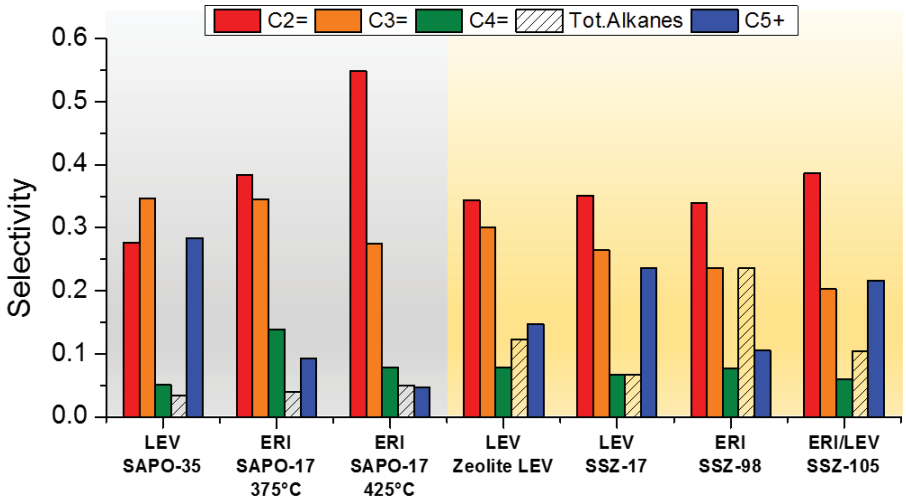

Figure 3.3. MTO product distributions when the methanol conversion is in the range of 98–100%. The selectivity data of SAPO-17 are reproductions of Wilson and Barger's work[44] and are obtained at T = 375 and 425 °C. The other reactions are performed at T = 400 °C and WHSV(MeOH) = 1.3 h^{-1}.

Category III Four isostructural AEI-type catalysts (SSZ-39, SAPO-18, CoAPO-18, and MgAPO-18) were prepared and their MTO reactions were investigated at the same reaction conditions. The product distributions of the AEI-series catalysts were illustrated in Figure 3.4 (a). The observed product distributions were in coherence with previous reports in the literature.[46, 67, 69, 88] Just like the CHA-series discussed above, the AEI-series also showed an impressive similarity regardless of elemental compositions. Again, these results solidly support the notion that it is the cage geometry that primarily determines the olefin product distributions. The overall alkane selectivity order (SAPO-18 < CoAPO-18 < MgAPO-18 < SSZ-39) can be results which were originated from differences among acid strength,[67, 88-89, 97] but any conclusive statement could not be made here because the acid site density was not controlled. The SSZ-39 shown in this work was synthesized from a sodium-free gel, inspired by a related work on SSZ-13 where the paired-site density was controlled

by modifying gel Na/OSDA ratios.[98] However, no discernable difference between this sodium-free SSZ-39 and conventional SSZ-39 synthesized from gel containing sodium hydroxide[69] was observed.

MTO product distributions of three high-silica zeolites (DDR, RTH, and ITE) having 5-membered rings as their structural component were shown in Figure 3.4(b). As explained in the previous section, these three zeolites showed olefin product distributions with predominant propylene selectivities, which is consistent with the literature.[32, 48, 99-100] The observed overall ethylene-to-propylene ratios of SSZ-28, zeolite RTH, and zeolite ITE were 0.62, 0.32, and 0.40, respectively. Corma et al. suggested that the RTH cage preferentially stabilizes fully substituted hydrogen pool intermediates which is responsible for its high propylene and butylene selectivity.[99] This is exactly opposite to the cases of SAPO-34 and LEV-type molecular sieves which prefer to possess partially substituted intermediates due to the spatial confinement effect.[33-34, 99]

Two STA-7 molecular sieves with different Si/T ratios gave very similar ethylene-to-propylene ratios. The overall ethylene-to-propylene ratios of STA-7(1) and STA-7(2) were 0.58 and 0.59, respectively. The SAV frameworks actually have two distinct cage structures. Here, only the major cage was considered because the minor cage is too small to accommodate any hydrogen pool intermediates. In terms of the diameter of the largest sphere which can occlude the cage, the minor cage of SAV (6.33 Å) is much narrower than an LEV cage (7.10 Å) or an ERI cage (7.04 Å), and slightly larger than an MTF cage (6.25 Å) or an ESV cage (6.22 Å) which are not capable of harboring aromatic hydrogen pool intermediate species.[87] Considering the known kinetic diameters of partially substituted benzene (o-xylene, 6.8 Å) or fully substituted benzene (hexamethylbenzene, 7.1–8.0 Å),[101] it is reasonable to assume that the minor cage of SAV plays a marginal role in hydrogen pool mechanism.

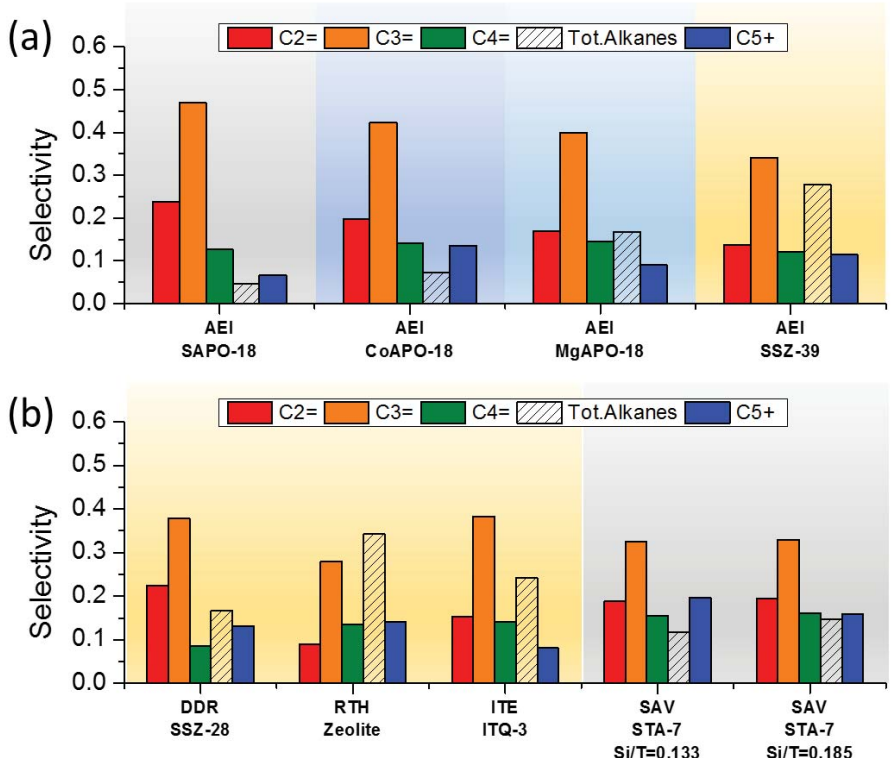

Figure 3.4. MTO product distributions when the methanol conversion is in the range of 98–100%: (a) four isostructural AEI-type molecular sieves, (b) three high-silica zeolites having DDR, RTH, and ITE-type topologies, and two SAPO materials having the SAV topology. The reactions are performed at T = 400 °C and WHSV(MeOH) = 1.3 h^{-1}.

Category IV The catalysts belonging to this category showed very complex patterns in terms of the ethylene-to-propylene ratio, as mentioned in the previous chapter. Unlike CHA, AFX, SFW, and AEI-type catalysts shown above, in this category, the influence of topology on ethylene-to-propylene ratios was weak. The high silica zeolite LTA gave an even-balanced ethylene-to-propylene ratio, while SAPO-42 clearly showed propylene-dominant product distribution patterns similar to those of SAV-type catalysts which belong to Category III. STA-14 gave a product distribution very similar to those of SAPO-42. The

similarity between STA-14 and SAPO-42 may be originated from their similar Si-distribution within frameworks caused by the use of the same OSDA (K222) for the formation of their LTA-cages. However, the KFI-type zeolite gave a very high ethylene-to-propylene ratio (1.59) which comes under Category II. Zeolite RHO also showed an ethylene-dominant product distribution, but the SAPO-material having RHO topology, DNL-6, showed a Category I-type ethylene-to-propylene ratio of 1.02. UZM-5 also showed an ethylene-to-propylene ratio (0.87) that is very close to unity.

The main cage structure of these four topologies is the same LTA cage having the same connectivity. But there are small differences among the cage sizes and 8-ring pore window dimensions due to the steric influence from secondary building units. In terms of the largest sphere that can be included in cavity, the size order is as follows: LTA (11.05 Å) > KFI (10.67 Å) > RHO (10.43 Å) > UFI (10.09 Å). The minor cages of UFI has a sphere diameter of 5.92 Å which is too small to contain hydrogen pool intermediate species. This size order has no correlation with the ethylene-to-propylene ratios. The sizes of these LTA cages are much larger than most of hydrogen pool intermediates such as hexamethylbenzene having a kinetic diameter of 7.1 Å.[101] So these cages may have weak limiting abilities that can control the side-chain lengths of small aromatic intermediates. Li and co-workers calculated the stabilization energies of carbonium ions with different lengths of side-chains (methyl, ethyl, isopropyl, and isobutyl) within the SAPO-35 (LEV), SAPO-34 (CHA), and DNL-6 (RHO) topologies.[33] Unlike the LEV and CHA cages, the LTA cage showed similar stabilization energies of large negative values for all type of intermediates due to the lack of steric hindrance, which implies no preference in side-chain lengths.[33] Thus, for the topologies of Category IV, the final MTO product distributions may be dependent more on secondary factors such as the acid-site distributions of cage walls. More experimental investigation is required on this topic. Although the catalysts in this category did not exhibit coherent behaviors in terms of the ethylene-to-propylene ratios, all of them produced distinctly high butylenes selectivities, which will be discussed in the next section.

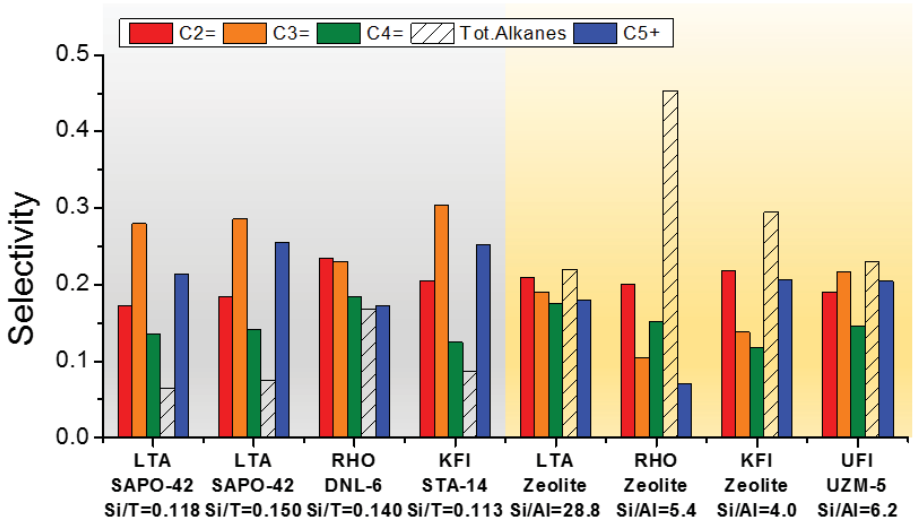

Figure 3.5. MTO product distributions of zeolites and SAPO-molecular sieves having LTA, RHO, KFI, and UFI-type topologies when the methanol conversion is in the range of 98–100%. The reactions are performed at T = 400 °C and WHSV(MeOH) = 1.3 h^{-1}.

3.2.2. Butylene Selectivity

Butylenes are another important products from the MTO reaction. There are many suggested pathways for the formation of butylenes (isomers of C_4 olefin). They can be formed from the pairing mechanism and/or side-chain mechanism in which hydrocarbon pool aromatics are involved.[9, 13] Propylene can also be upgraded to butylenes by reacting with methanol and/or by cracking of higher olefins in the alkene cycle.[8] The suggested mechanistic pathways that yield butylenes are illustrated in Figure 3.6. Though the elucidation of the origin of C_4 olefin formation mechanism is out of the scope of this work, the correlation between the cage structures and the observed butylenes selectivities could be established from the experimental results of this work.

On the GC-MS chromatograms (not shown) all four isomers of butylenes (1-butene, trans-2-butene, cis-2-butene, and isobutene) could be detected from the MTO reaction effluents. However, on chromatograms, peaks of these C_4 olefin isomers were partially overlapped with those of saturated C_4 paraffin isomers (n-butane and isobutane). For this practical reason, in this work, the integrated (sum) selectivity of all butylene isomers were evaluated. The contribution of overall butylene selectivity in final olefin product distributions was quantified on the basis of the ratio ($2S_B/(S_E+S_P)$) of overall butylene selectivities (S_B) to the average of ethylene and propylene selectivities ($(S_E+S_P)/2$). This ratio is denoted as *the butylene contribution ratio* here. The butylene contribution ratios of all MTO catalysis runs were displayed in Figure 3.7 together with the ethylene-to-propylene ratios.

As mentioned in the previous section, all four members (LTA, RHO, KFI, and UFI) of Category IV gave very high butylene selectivities. The butylene contribution ratios of these catalysts were similar to or higher than 0.5 regardless of their elemental compositions, as shown in Figure 3.7. Zeolite RHO (0.99), High-silica zeolite LTA (0.87), and DNL-6 (0.73) gave the highest butylene contribution ratio among all tested catalysts. Interestingly, the latter two catalysts showed almost even-balanced selectivity ratios across ethylene, propylene, and butylenes. (*i.e.*, ca. ethylene:propylene:butylene = 1:1:1) The lowest butylene contribution ratio among Category IV was observed from STA-14 (0.49). However, this value is still higher than most of the catalysts from the other categories, such as SAPO-34 (0.29) or SAPO-18 (0.36). Pinilla-Herrero et al.[39] and Li et al.[33] also previously reported high butylenes selectivities from SAPO-42 and DNL-6, respectively. Pinilla-Herrero and co-workers suggested that the high butylenes selectivity observed from SAPO-42 could be due to the wide pore of LTA (4.1 × 4.1 Å).[39] However, this theory cannot explain the high butylene selectivities observed from the RHO-type catalysts that have pore openings (3.6 × 3.6 Å) narrower than SAPO-34 (3.8 × 3.8 Å).

Some of the catalysts from the other categories also gave high butylene selectivities. Based on the butylenes contribution ratio, the following topologies yielded high butylene selectivities other than the Category IV catalysts: AFX, SFW, SSZ-104, and all Category III catalysts except for DDR. One thing in common among these topologies is the sheer size of the cage. AFX and SFW have large and elongated cages. SSZ-104 has intergrown GME domains which can provide large spaces within its 12-ring large-pore channels. DDR has the smallest cage among the Category III catalysts. Unlike ethylene and propylene, it can be concluded that the butylene selectivity seems to have a relationship with the volume of cages. Wider cages may be able to provide extra spaces for other mechanisms of MTO reaction such as the alkene cycle, but it was not investigated in this work.

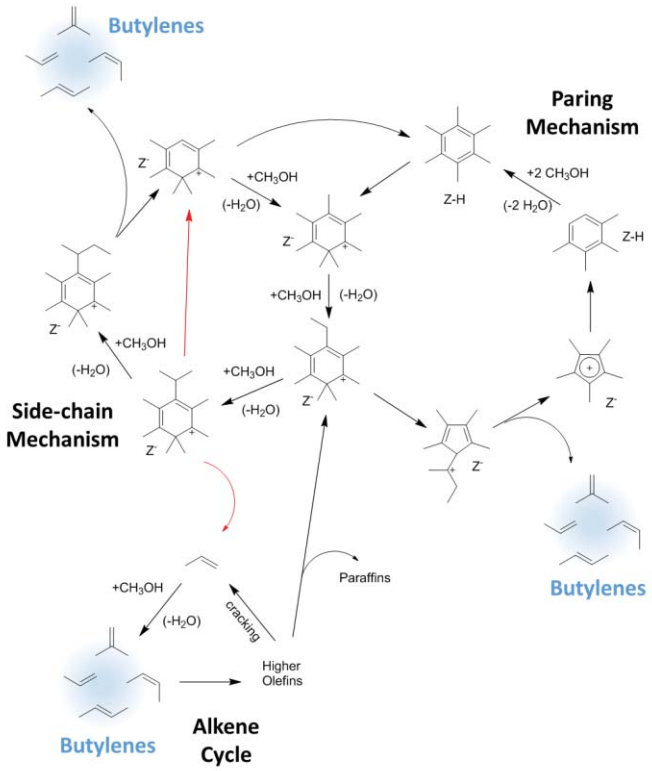

Figure 3.6. Suggested mechanistic pathways for the formation of butylenes. Z-H and Z^- refer to the zeolite Brønsted acid site and its conjugate base, respectively.

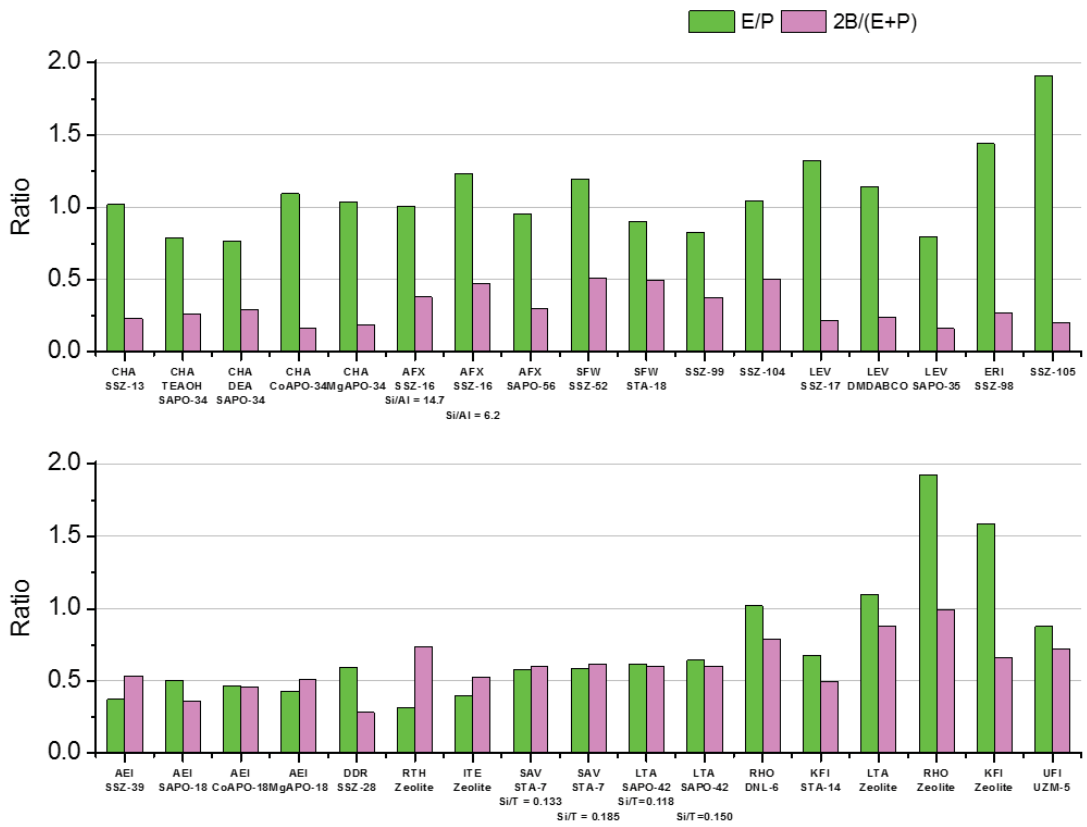

Figure 3.7. Ratios of light olefin selectivities (E; ethylene, P: propylene, B: butylenes) of all catalysts investigated in this work. All reactions are performed at 400 °C and WHSV(MeOH) = 1.3 h^{-1}.

3.2.3. Initial Propane Selectivity

From the MTO reactions, not only light olefins but also small paraffins (ethane, propane, and butanes) are obtained as co-products. The majority of these alkane products is propane which takes up more than 80 % of total alkane selectivities. In the fixed-bed reactors, most of propane formed from the methanol conversion is observed at the very initial stage

(time on stream < 15 min, g_{MeOH}/g_{cat} < 0.33) of reaction. From the most of time of stream data shown in the previous chapter, particularly for zeolites, high total alkane selectivities (in fact, mostly propane) are observed in the initial stages of methanol injection. The formation of this 'initial propane' has been linked to the formation of polyaromatic species within cages.[27-28] Later, it was found that the formation of alkanes is involved in the cyclization of higher olefins into aromatic hydrogen pool intermediates in the dual-cycle mechanism in ZSM-5.[30, 102-103] The initial propane selectivity itself has a strong correlation with the acid strength and acid-site density.[102, 104-105] Deimund et al. reported that there is a strong correlation between the acid site density in SSZ-13 and the initial propane selectivity,[87] and similar trends were also observed in this work from LEV- and AFX-type zeolites.

The observed initial propane selectivity values taken at the initial stage (TOS = 7–9 min) of the methanol injection from all zeolites and SAPO-based catalysts were plotted with respect to the heteroatom concentration (Figure 3.8). Apparently, zeolites generally yielded more initial propane than SAPO-based catalysts. The initial propane selectivity from various zeolites spanned even over 70 % depending on the topology and Si/Al ratio, while the highest propane selectivity for SAPOs was observed from STA-18 (19.5 %) having an SFW topology. Considering the fact that SAPO-based molecular sieves generally have milder acid sites than the isostructural zeolites, this result is consistent with the previous study which concluded that catalysts with stronger acid sites yield more initial propane.[105]

Interestingly, the topology was another important factor that determines the initial propane selectivity. Generally, large and wider cages gave more initial propane. For zeolites, the initial propane order was SFW, AFX > AEI, RTH, LTA, RHO > CHA > LEV, ERI. The SAPO-based catalysts showed a roughly similar trend: SFW > RHO > AFX > SAV > CHA, KFI > LTA > LEV. In both zeolite and SAPO systems, SFW-type catalysts yielded the highest initial propane selectivities, and LEV-type catalysts gave the least amounts of initial propane regardless of elemental composition. Given that the SFW is one of the largest cages

among the tested topologies and that LEV is the smallest one, it can be concluded that the initial propane selectivity has a significant relation with the cage size.

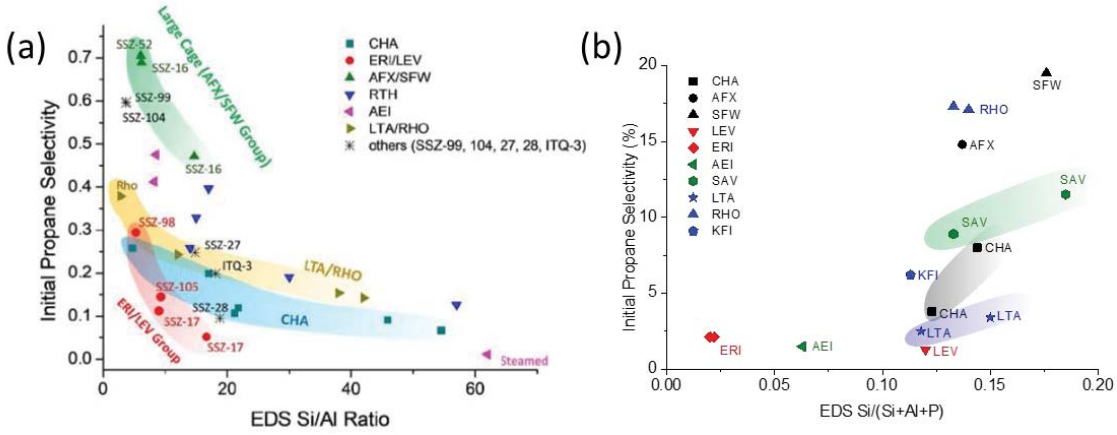

Figure 3.8. Effects of heteroatom concentration (Al in zeolites, and Si in SAPOs) and topology on the initial propane selectivities (time on stream = 7–10 min) of catalysts: (a) zeolites and (b) SAPOs. Some of the initial propane data points of SSZ-17 (Nu-3),[41] zeolite RTH,[48] zeolite LTA,[62] zeolite RHO,[106] SSZ-13,[64] and SSZ-39[69] are reproduced from articles previously published by our research group.

3.3. Concept of Cage-Defining Ring

3.3.1. Basic Idea and Development of Concept

A lesson from the large collection of data provided here is that the topology is the most important factor that primarily determines the final MTO product distributions at a fixed temperature. In this section, a new structural indicator that can be used to characterize these topologies will be introduced.

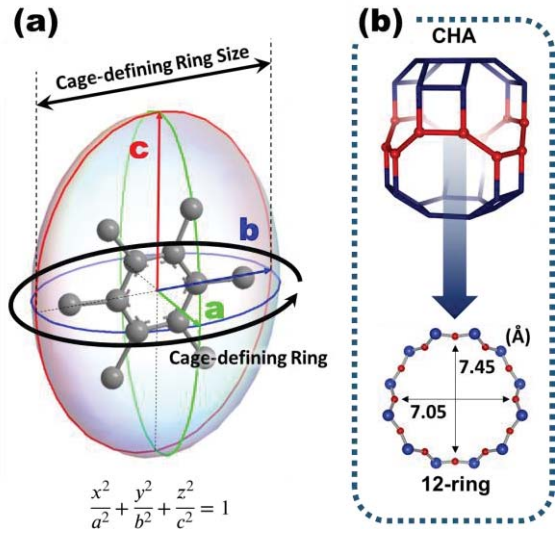

Figure 3.9. Determination of the cage-defining ring. (a) A hypothetical ellipsoidal model for the cage-defining ring and its size. (b) Selection of cage-defining ring from a CHA cage.

Unlike simple cylinders or ellipsoids, real zeolitic cages have very 'non-linear' shapes which cannot be easily explained by heights, widths, lengths, and volumes, as shown in Figures A1–A8. To find out the most important geometric parameter, a hypothetical model cage that has an ideal ellipsoidal shape with which is easy to deal is considered. An ellipsoid is defined by its three primary axes, *a*, *b*, and *c* where $a \leq b \leq c$. As a thought experiment, a planar aromatic molecule which represents a hydrogen pool intermediate (*e.g.*, hexamethylbenzene) is inserted in the ellipsoidal cage. The preferred orientation for the planar molecule will be being parallel to the *bc* plane and perpendicular to the *a* axis since it is the most energetically favorable orientation that maximizes the molecule-framework interaction. Figure 3.9(a) illustrates an aromatic molecule having such orientation within an ellipsoidal cage. One can easily notice that the limiting dimension for the size of the occluded

aromatic molecule is the second longest axis *b*. The shortest axis *a* and the longest axis *c* is less important in this view. In this model, the ellipse *ab* and the length of second-longest axis *b* were defined as *the cage-defining ring* and *the cage-defining ring size*. In the following section, how this concept can be applied to the real cages will be explained.

3.3.2. Selection of Cage-Defining Rings and Four Categories

Selecting cage-defining rings from real cages is essentially analogous to the procedure explained in the previous section for a hypothetical ellipsoidal cage, but is on the basis of the crystallographic data (*e.g.*, *.cif files) which can be obtained from the IZA database or elsewhere.[16] For real cages, there are many choices for rings composed of tetrahedral atoms and oxygens. Among them, the smallest ring which is closest to the center of mass of the cage was selected. This is the cage-defining ring of the cage and corresponds to the ellipse *ab* of the ellipsoidal model shown in Figure 3.9(a) and explained in the previous section.

Figure 3.9(b) describes the case of a CHA cage as an actual example. In the case of CHA, the 12-membered ring that encircles the 'waist' of the cage which is perpendicular to the c axis is the cage-defined ring (red-colored ring in Figure 3.9.(b)). The dimension of this ring can be easily measured in the same matter as when measuring channel dimensions in zeolites. In this manner, the dimension of the selected 12-membered ring (cage-defining ring of CHA) is 7.45 × 7.05 Å. And finally, the longer axis of this ring (7.45 Å) is what we denote as the cage-defining ring. Tetrahedral atoms and oxygen atoms are assumed as hard spheres having a diameter of 2.7 Å in accordance with the IZA convention.[16] The same selection procedures were undergone, and the results were summarized and visualized in Table 3.1 and Figures A1–A4.

Finally, the correlation between the cage-defining ring sizes and the four categories of topologies (on the basis of olefin product distributions) was illustrated in Figure 3.10. Firstly, the three frameworks of the Category I (CHA, AFX, SFW) have 12-membered cage-defining rings, and their cage-defining ring sizes are almost equal (7.45 Å). This is because these topologies are members of the AABBCC-6 family that is closely related to the GME framework. In the previous section, it was shown that the ethylene-to-propylene ratios from the MTO reactions of CHA, AFX, and SFW-type catalysts were close to unity regardless of cage lengths and elemental compositions. The two Category II topologies (LEV and ERI) also have 12-membered cage-defining rings, but their sizes are smaller than 7.45 Å. Catalysts of Category II yielded high ethylene selectivities. The members of Category III have 14-membered cage-defining rings except for DDR which is only one exception. Catalysts having Category III topologies gave propylene-dominant product distributions without exception as shown in the previous section. DDR have a 12-membered cage-defining ring like Category I and II materials, but yielded higher propylene selectivities than ethylene. This is because of the fact that the cage-defining ring had to be selected away from the center of mass of the cage due to the positions of pore openings of a DDR cage. A DDR cage is actually wider than a CHA cage on the basis of the maximum included sphere diameter (DDR: 7.66 Å; CHA: 7.37 Å) and the tree-ring plot shown in Figure A7. Lastly, all four topologies belonging to Category IV have 16-membered cage-defining rings since all of them have LTA-cages of the same connectivity. The cage-defining ring sizes of these cages were larger than 10 Å. Again, as illustrated in Figure 3.10, the cage-defining ring sizes and the four categories based on olefin product distributions show an exceptionally strong correlation.

Table 3.1. Topological information of small-pore frameworks investigated in this work.

Framework	Channel Dimension	Framework Density (nm^{-3})	Maximum Sphere (Å) †	Pore Window (Å)	Diffusing Max. Sphere (Å)	Cage-Defining Ring Size (Å)
CHA	3	15.1	7.37	3.8 × 3.8	3.72	7.45
AFX	3	15.1	7.76	3.6 × 3.4	3.73	7.44
SFW	3	15.1	7.78	4.1 × 4.1	3.65	7.45
LEV	2	15.9	7.10	4.8 × 3.6	3.53	7.15
ERI	3	16.1	7.04	5.1 × 3.6	3.42	6.76
DDR	2	17.9	7.66	4.4 × 3.6	3.65	7.07
AEI	3	15.1	7.33	3.8 × 3.8	3.84	8.52
RTH	2	16.1	8.18	4.1 × 3.8 5.6 × 2.5	4.14	9.00
ITE	2	15.7	8.30	4.3 × 3.8 5.8 × 2.7	4.21	9.11
SAV†	3	14.6	8.82	3.9 × 3.9 3.8 × 3.8	4.10	9.60
LTA	3	14.2	11.05	4.1 × 4.1	4.21	10.44
RHO	3	14.5	10.43	3.6 × 3.6	4.06	11.41
KFI†	3	15.0	10.67	3.9 × 3.9	4.04	10.16
UFI†	2	15.2	10.09	4.4 × 3.6 3.3 × 3.3	3.89	10.45

† For topologies having two or more cage structures (SAV, KFI and UFI), only the major cage (largest cage) was considered. All crystallographic data were obtained from the IZA database.[16]

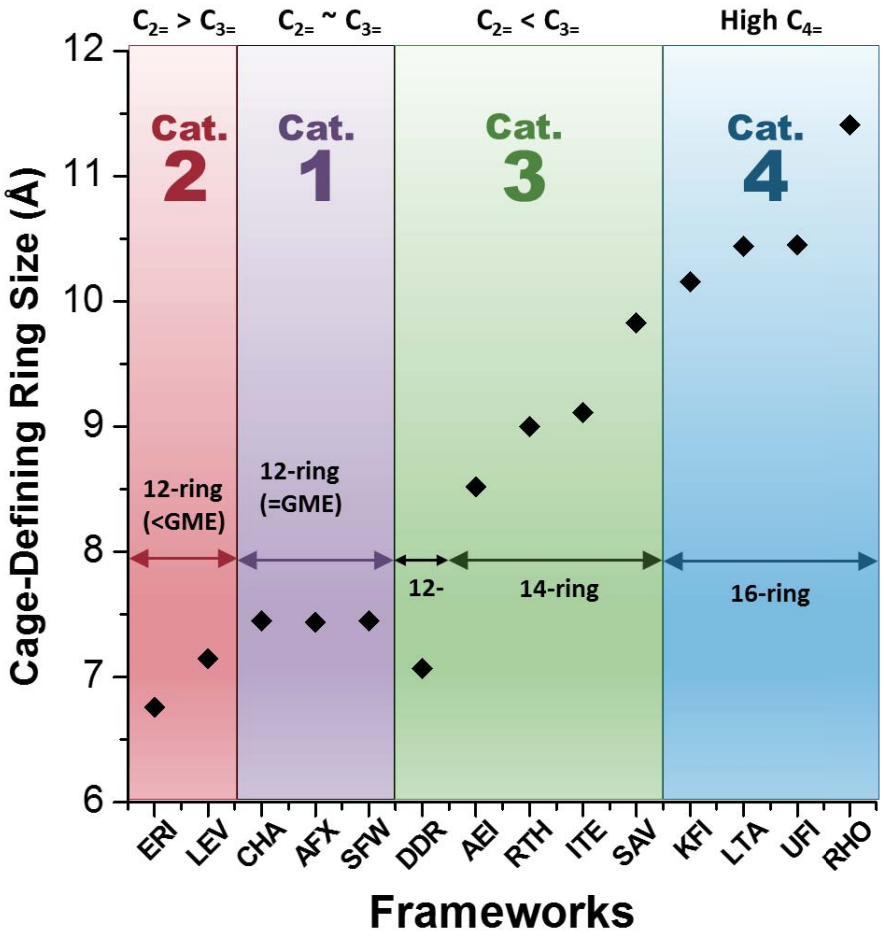

Figure 3.10. Correlation diagram between four categories of topologies and cage-defining ring sizes.

3.4. Summary

The MTO product distributions from 30 MTO catalysts from 14 different topologies were investigated in respect of overall product selectivity patterns in the range of full methanol conversion. This may be the most extensive collection of MTO reaction data from different topologies and elemental compositions which has ever been reported up to date.

The notion that it is the topology that primarily dictates the final olefin product distributions was confirmed. Based on a simple model of hypothetical ellipsoidal cage, the concepts of cage-defining ring and cage-defining ring size were established. The cage-defining ring size showed a strong correlation with the four categories of topologies. Finally, the descriptions of the four categories based on the MTO product selectivity distributions could be augmented with the concept of cage-defining ring, as follows:

At the MTO reaction temperature of 400 °C,

- Category I: group of CHA, AFX, SFW, SSZ-99, and SSZ-104 which show even-balanced ethylene-to-propylene ratios close to unity (E/P ~ 1). Members of this category had 12-membered cage-defining rings. Their cage-defining ring sizes were similar to the dimension of the 12-membered main channel of GME (~ 7.45 Å).
- Category II: group of LEV, ERI, and SSZ-105 which show ethylene selectivities higher than propylene selectivities (E/P > 1). Members of this category had 12-membered cage-defining rings. Their cage-defining ring sizes were narrower than those of Category I (< 7.45 Å).
- Category III: group of DDR, AEI, RTH, ITE, and SAV which show propylene selectivities higher than ethylene selectivities (E/P < 1). Members of this category had 14-membered cage-defining rings except for DDR having a 12-membered cage defining ring. Their cage-defining ring sizes were narrower than those of Category I (> 7.45 Å).
- Category IV: group of LTA, RHO, KFI, and UFI which show no clear pattern of ethylene-to-propylene, but high butylenes selectivities with the LTA cages as their major cages in common. Members of this category had common 16-membered cage-defining rings. Their cage-defining ring sizes were the widest (> 10 Å).

Relevant supplementary visualizations which helps readers to ‘get the feel of’ real sizes of cages were provided in Appendix A. The cage-defining ring is a reliable metric that

connects the cage structures to the final product distributions. This geometric indicator based on the intermediate shape selectivity can be directly obtained from the most of common types of crystallographic information of topologies such as the *.cif files. Even from a novel structure having a small-pore/cage-type topology which has never been tested before, the final MTO product distributions can be predicted only based on the crystallographic information without performing sophisticated computations. I believe that this concept of cage-defining ring will provide guidance for further investigation of MTO reactions regarding the shape selectivity of cage structures.